JCB Article

Slow local movements of collagen fibers by fibroblasts drive the rapid global self-organization of collagen gels

Ravi K. Sawhney[1,2] and Jonathon Howard[1,3]

[1]Max Planck Institute of Molecular Cell Biology and Genetics, 01307 Dresden, Germany
[2]Molecular and Cellular Biology Program and [3]Department of Physiology and Biophysics, University of Washington, Seattle, WA 98195

A classic model for tissue morphogenesis is the formation of ligament-like straps between explants of fibroblasts placed in collagen gels. The patterns arise from mechanical forces exerted by cells on their substrates (Harris et al., 1981). However, where do such straps come from, and how are slow local movements of cells transduced into dramatic long-distance redistributions of collagen? We embedded primary mouse skin and human periodontal ligament fibroblasts in collagen gels and measured the time course of patterning by using a novel computer algorithm to calculate anisotropy, and by tracking glass beads dispersed in the gel. As fibroblasts began to spread into their immediate environments, a coordinated rearrangement of collagen commenced throughout the gel, producing a strap on a time scale of minutes. Killing of cells afterwards resulted in a partial relaxation of the matrix strain. Surprisingly, relatively small movements of collagen molecules on the tensile axis between two pulling explants induced a much larger concomitant compression of the gel perpendicular to the axis, organizing and aligning fibers into a strap. We propose that this amplification is due to the geometry of the collagen matrix, and that analogous amplified movements may drive morphological changes in other biological meshes, both outside and inside the cell.

Introduction

Movements of cells are usually studied in the context of the four-step cycle of cell migration: extension, attachment, contraction, and detachment (Bray, 2001). A cell extends, attaches to its two-dimensional substrate or three-dimensional matrix, contracts, and thus exerts a traction (drawing) force on its surroundings. At that point, if the rear of the cell detaches from the substrate, the cell is drawn forward: this is migration. If the detachment step is omitted, the end product of the three-step cycle is the traction force, which then might draw in the surrounding matrix. We will refer to all movements of substrate or matrix, resulting from traction forces not expressed as cell migration, simply as traction. Traction results in strain within the matrix, which may serve an important role in tissue morphogenesis and homeostasis. Some cells seem to be specialized for either traction or migration. Fibroblasts, which migrate slowly, display large traction effects, distorting their substrates far more than do faster-migrating cells such as leukocytes and keratocytes (Harris et al., 1981; Fray et al., 1998). With cultured fibroblasts, traction can wrinkle rubber substrates (Harris et al., 1980) or condense collagen matrix around the body of the cell (Yamato et al., 1995). When populations of fibroblasts are dispersed in collagen matrix, a loose collagen gel tethered at its edges can be pulled into tension (Bellows et al., 1981; Eastwood et al., 1994), or an untethered gel can be drawn into a tight knot (Bell et al., 1979). Most remarkably, A.K. Harris and colleagues (1981) embedded two tissue explants more than a millimeter apart in a collagen gel and showed that after 2–4 d, traction by the explant fibroblasts had combined to produce a ligament-like strap on the axis between the explants. The pattern of aligned collagen implied that traction may also be important in vivo, providing the driving force behind the patterning of collagen in connective tissues during development and wound healing (Bellows et al., 1982; Stopak and Harris, 1982).

Great progress has been made toward understanding the individual cellular and molecular mechanisms that underlie traction. The dynamics of actin assembly during extension has been directly visualized (Wang, 1985; Theriot and Mitchison, 1992), key molecules that regulate actin assembly have been isolated and reconstituted (Machesky et al., 1994; Loisel et al., 1999; Svitkina and Borisy, 1999), substrate attachment has been followed in real time (Kaverina et al., 1999; Anderson and Cross, 2000), and the forces associated with cell contraction have been measured (Lee et al., 1994; Galbraith and Sheetz, 1999; Balaban et al., 2001; Beningo et

The online version of this article contains supplemental material.

Address correspondence to Jonathon Howard, MPI-CBG, Pfotenhauerstrasse 108, 01307 Dresden, Germany. Tel.: 49-351-210-2500. Fax: 49-351-210-2020. E-mail: howard@mpi-cbg.de

Key words: traction; morphogenesis; anisotropy; fibroblasts; collagen

Supplemental material can be found at:
http://doi.org/10.1083/jcb.200203069

al., 2001). The effect of these forces on the tension and density of surrounding substrate have also been well characterized (Guidry and Grinnell, 1985; Brown et al., 1998).

However, little progress has been made toward understanding how these individual components might combine to result in the large-scale anisotropic patterning seen in vitro by Harris et al. (1981), and in vivo during tissue morphogenesis. The lack of progress may stem from two apparent discrepancies of scale—temporal and spatial—between traction patterning and its cellular components. First is the temporal discrepancy. The cell motility machinery driving migration and presumably traction operates on a timescale of minutes: extension of the leading edge occurs at rates up to 1.5 μm/min (Theriot and Mitchison, 1992), the majority of adhesive contacts have a lifespan of <30 min (Kaverina et al., 1999), and centripetal movement of these contacts due to contraction occurs at rates up to ~0.5 μm/min (Smilenov et al., 1999). These rates accord with the migration of fibroblasts at 0.5–1.0 μm/min (Vasiliev et al., 1970; Harris et al., 1981). On the other hand, there is a general conception that tissue patterning is a much slower process operating on a time scale of days (Smilenov et al., 1999). If traction and migration are indeed driven by the same basic mechanisms, then traction and migration should occur on similar timescales, namely minutes, and the substrate movement involved in patterning should occur at a speed similar to that of fibroblast migration. However, if the time scales are indeed similar, then there is a spatial discrepancy: how could the small collagen movements produced by a fibroblast moving at 0.5 μm/min induce, within minutes, a pattern of dimensions >1 mm?

Here we show that traction patterning does indeed occur on a timescale of minutes, with small movements of cells inducing a near-concomitant coordinated reorganization of the collagen gel. The efficiency of the patterning arises from the mechanical integration of the collagen fibers into a mesh. We present a model describing how the geometric properties of such biological meshes may guide a variety of molecular morphogenetic movements, both outside and inside the cell.

Results

The time course of traction patterning

In order to determine the time course of patterning we modified Harris et al.'s (1981) model system by adding a novel computer algorithm for measuring the developing anisotropy of collagen matrix. Explants, groups of trypsinized mouse dermal and human periodontal ligament fibroblasts, were embedded ~1 mm apart in 1.7-mg/ml type I collagen gels and observed by phase contrast video microscopy. Initially, the collagen gel was a coarse isotropic mesh of fine phase-dark fibers, and the cells were spherical due to their recent trypsinization (Fig. 1 A). After ~1 h , the cells began to extend processes into the gel, deforming the adjacent collagen fibers. Over the next several hours, striated regions, which we call straps, formed between the explants (Video 1, available at http://www.jcb.org/cgi/content/full/jcb.200203069). These regions contained thick collagen fibers aligned parallel to the axes between explants (Fig. 1 B). Because of the variability in the time that it took for cells to recover from trypsinization and transfer, time 0 in each experiment was defined as the time at which a process longer than 10 μm was first observed. Time 0 was always within 90 min of cell plating, and usually corresponded to the spread of only 2 or 3 cells out of a field of hundreds, indicating that our analysis did not miss any substantial cell activity. Analysis of individual fibroblasts spreading on glass and in collagen gels indicated that such a 10-μm-long process takes ~10 min to grow; therefore, we consider time 0 to be within 10 min of the time when the first cells recover and are able to conduct rudimentary motility.

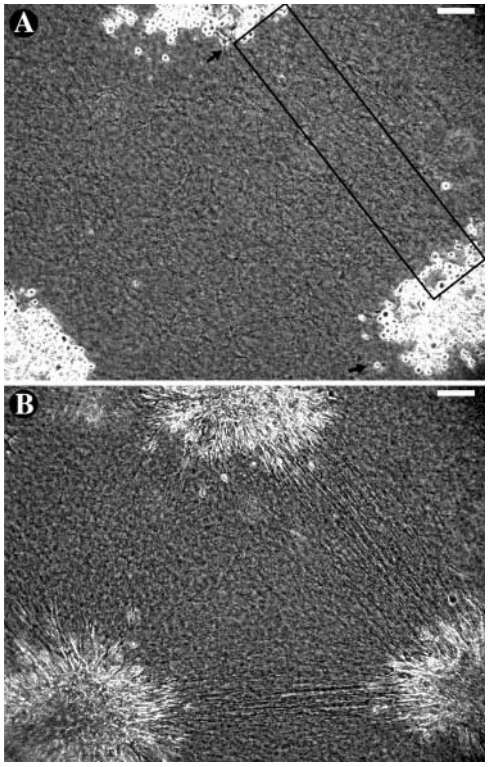

Figure 1. **Mouse dermal fibroblasts pattern a collagen gel.** (A) At time 0, collagen appeared as a coarse isotropic mesh and traction-type motility first started (arrows). The boxed region is expanded in Figure 2. (B) Over 8 h, explants took on a starburst appearance and traction-aligned straps formed between them. The lack of strap formation between the upper and lower left explants may be due to the 250-μm shift of the lower left explant from its initial position or the effect of an explant up and to the left (unpublished data). Bars, 100 μm. (See Video 1, available at http://www.jcb.org/cgi/content/full/jcb.200203069.)

Straps were apparent to the eye within 3 h (Fig. 2 A). However, computer analysis revealed that the long-range rearrangement of collagen fibers underlying the strap began much earlier. The time course of pattern formation was measured by an algorithm that calculated the anisotropy of the developing strap (see Materials and methods). For each image, the region between explants was digitally sliced into lines both parallel and perpendicular to the forming strap. In the mature strap, lines parallel to the strap tended to be either all light or all dark due to the alignment of collagen, and were therefore of low contrast. Lines cutting across the strap traversed light and dark regions and were therefore of

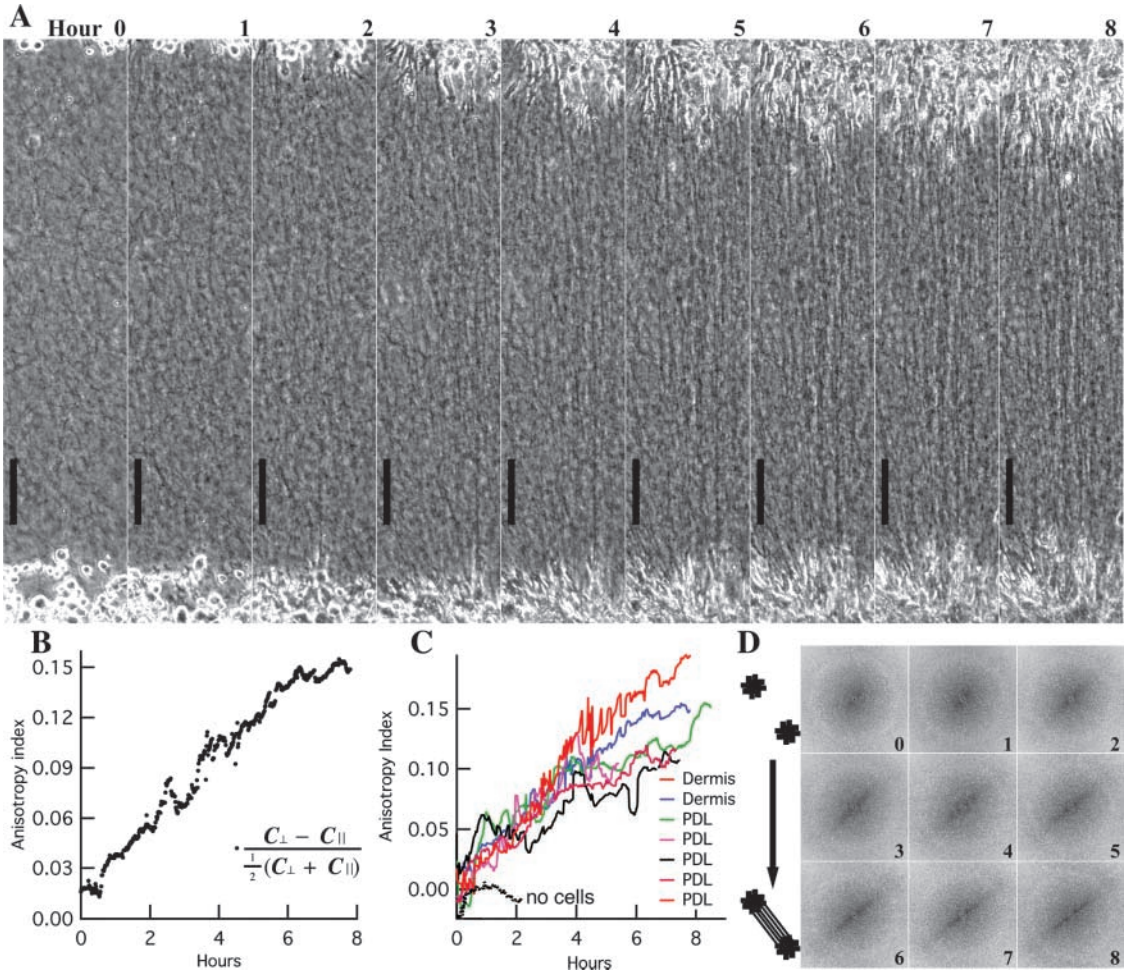

Figure 2. **Analysis of pattern.** (A) Hourly images from Fig. 1 experiment (rotated). The strap pattern became obvious to the eye by hour 3. (B) Contrast analysis revealed that anisotropy began to rise within 30 min and continued to rise over 7 h. (C) With mouse dermal and human periodontal ligament fibroblasts, anisotropic straps began to emerge at 6 ± 15 min; no alignment occurs without cells. (D) Power density spectra (unrotated) from Fourier transformations became anisotropic over time. The increase in high frequency signal perpendicular to the strap indicates that fibers became packed more closely parallel to the strap. Bars, 100 μm.

higher contrast. The relative difference between perpendicular and parallel contrasts served as an index of anisotropy. The contrast anisotropy was measured every minute.

Initially, the anisotropy index was near zero (Fig. 2 B), confirming that the matrix was isotropic prior to cell spreading. Within 30 min, the anisotropy index began to rise and it continued to rise for the following 8 h as the strap pattern emerged. An increase in the anisotropy index was observed in all gels containing either mouse dermal fibroblasts or human periodontal ligament fibroblasts, but not in gels containing no fibroblasts (Fig. 2 C). The rising anisotropy of the gel was also demonstrated by Fourier analysis: the two-dimensional power density spectra were initially radially symmetric but became compressed along the frequency axis perpendicular to the axis of the forming strap (Fig. 2 D).

In the presence of fibroblasts, the rise in anisotropy was evident within minutes. Polynomial curves fit to the anisotropy indices (Fig. 2 C) over the first 300 min indicated an average onset time of +6 ± 15 min (mean ± SD) for six straps (one strap, corresponding to the green curve, was not included in the average because its data were very noisy and the apparent onset time of –153 min was >10 SDs away from the mean time for the other straps). Therefore, we conclude that the onset of patterning was not significantly different from the onset of fibroblast spreading. We have 95% confidence that the delay between the first signs of cell motility and pattern formation is <30 min (mean + 2 SEM + 10 min between motility and spreading).

The rise in anisotropy occurred uniformly throughout the region between the explants. This was evident in the hourly still images (Fig. 2 A) and was confirmed by dividing the time-lapse series of rectangular images of the strap region along its length into six subregions and performing contrast analysis on each subregion individually. Comparing the central subregions to the subregions near the explants, there was no significant difference in either the time of onset or the slope of the rise in the anisotropy index. This indicated that the pattern did not progress or creep from the explants toward the center; instead, the alignment emerged simultaneously all along the strap. Thus, the anisotropy index is a measure of the collagen pattern forming throughout the strap, and this pattern emerges on a time scale of minutes, essentially simultaneously with the onset of cell spreading.

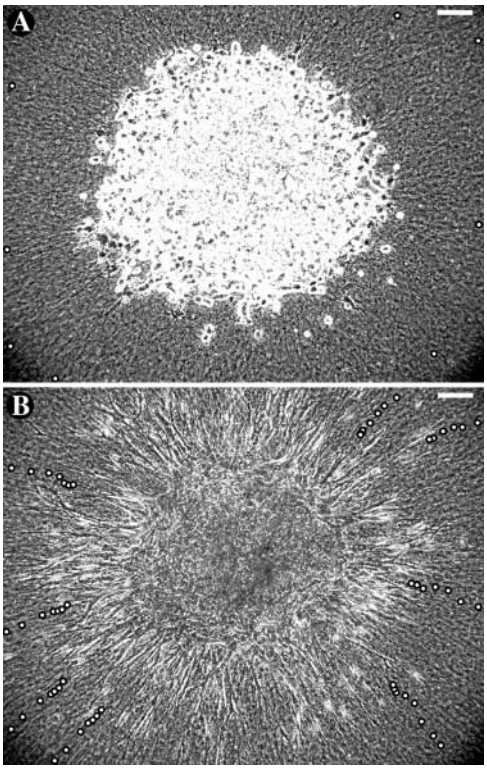

Figure 3. **Centripetal movements of collagen toward explant.** A solitary explant of human periodontal ligament fibroblasts was placed in the center of a dish of collagen with fiducial glass spheres. (A) Initial positions of eight beads to be tracked are marked with white circles. (B) Bead positions at 3-h intervals are shown in the final image, taken after 18 h. Comparing the areas of concentric circles connecting the eight initial and eight final beads revealed that over 18 h, the collagen content of the explant area approximately doubled (assuming no degradation). Bars, 100 μm. (See Video 2, available at http://www.jcb.org/cgi/content/full/jcb.200203069.)

Cell and matrix movements that drive patterning

Fibroblasts are slow, so the rapidity of the onset of patterning suggested that only small movements of cells and their associated collagen are required to establish the pattern. In order to calculate the minimum distance that collagen fibers must be translocated by the explants during the initial formation of the pattern, we measured the speed at which the fibers move. Towards this end, a solitary explant of human periodontal ligament fibroblasts was embedded in collagen and observed over 18 h (Fig. 3). Without an opposing explant, matrix was towed in symmetrically from all directions, at its maximal rate. Glass beads were dispersed at the cell layer of the gel, where they remained stationary relative to local collagen architecture. Their brightness in phase contrast enabled accurate tracking of movements of collagen fibers nearby. At the onset of filming, cells were mostly round, although a few had already begun to elongate and align collagen radially. In time-lapse video (Video 2, available at http://www.jcb.org/cgi/content/full/jcb.200203069), the explant took on a starburst appearance as fibroblasts extended outward from the explant. Fibroblast motility was persistent and directed centrifugally throughout the experiment. The cells extended to as long as 200 μm and could be seen advancing through collagen, but little net migration (progress of cells away from the center of explant) occurred because the matrix was simultaneously being towed back toward the explant (Table I). Over the first 6 h, collagen moved centripetally at an average of 0.28 ± 0.06 μm/min (mean ± SD). During this time, cell bodies at the edge of the explant were transported inward as well as matrix, thus drawing the explant into a dense clump studded with advancing cell processes. These processes, as if on a treadmill, departed the explant at a speed similar to that at which collagen was carrying them back in. Therefore, the leading edges of most cells remained nearly stationary with respect to the view of the microscope over the first 6 h, advancing at only 0.08 ± 0.12 μm/min.

Collagen movement toward the explant slowed with time, as demonstrated by the closer relative spacing of the later tracking points in Fig. 3 B. The average inward speed of the beads decreased to 0.15 ± 0.03 μm/min during hours 7–12 and then to 0.08 ± 0.02 μm/min during hours 13–18. To confirm that the decrease in speed was time dependent, rather than dependent on proximity to the explant, beads that came into view at the periphery of the image were tracked between hours 13 and 18. They showed a similarly slow rate of movement, 0.07 ± 0.03 μm/min, indicating a global decrease in matrix traction (progress of collagen toward the center of the explant). As the matrix slowed, cell advancement away from the clump accelerated. During hours 13–18, advancing cell processes left the explant at 0.29 ± 0.08 μm/min. Once the speed of cell migration surpassed the speed of matrix traction at around hour 6, the clump expanded in diameter steadily until the end of the experiment. Subtracting the backward speeds of the beads from the forward speeds of the advancing cells revealed that matrix was moved along the cells at a consistent rate of 0.36–0.41 μm/min throughout the experiment.

Table I. **Cell and matrix movements surrounding single explant**

	Absolute speed of beads	Absolute speed of advancing cell processes	Speed of advancing cell processes relative to beads
	μm/min ± SD (n)	*μm/min ± SD (n)*	*μm/min ± SD (n)*
Hours 1–6	−0.28 ± 0.06 (8)	+0.08 ± 0.12 (11)	+0.36 ± 0.13
Hours 6–12	−0.15 ± 0.03 (8)	+0.26 ± 0.07 (7)	+0.41 ± 0.08
Hours 12–18		+0.29 ± 0.08 (7)	+0.37 ± 0.08
Near explant	−0.09 ± 0.02 (8)		
Peripheral	−0.07 ± 0.03 (6)		

Speeds of beads and advancing cell processes were measured relative to the microscope field; positive values indicate movements away from the explant. The inward movement of the matrix was initially rapid, bringing with it cells at the explant boundary. Therefore, outward advancing cell processes achieved little net progress over the first 6 h. Matrix movements slowed with time, both near the explant and at the periphery of the field of view. As the matrix slowed, the cells accelerated, maintaining a constant translocation speed with respect to the matrix.

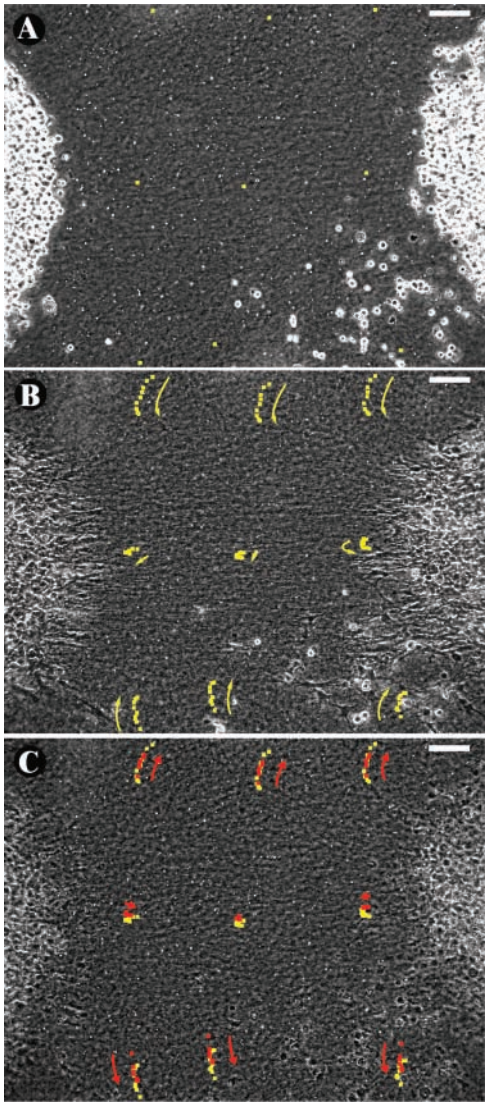

Figure 4. **Collagen rearrangements during strap patterning.** Two explants of human periodontal ligament fibroblasts embedded in a collagen gel with scattered glass beads. (A) Initial positions of beads to be tracked are shown. (B) Bead positions at 1-h intervals (yellow). Bead movements indicate that traction resulted in a small (<5%) strain on the axis between explants. More dramatic movements occurred adjacent to the strap, where collagen was drawn laterally towards the axis. (C) Maitotoxin induced a release of 1/2 to 2/3 of the matrix deformation as revealed by bead positions at 10 min intervals (red). Bars, 100 μm. (See Video 3, available at http://www.jcb.org/cgi/content/full/jcb.200203069.)

From the initial rate of collagen traction (0.28 μm/min) and the time it takes the pattern to start forming (<30 min), we can now estimate that collagen translocation of <10 μm at the surface of the explant is sufficient to evoke the observed rearrangement of matrix over a span of 1,000 μm, the size of a strap.

Matrix movements during strap formation

It seemed remarkable that such a small movement of collagen fibers could organize the gel into a structure more than two orders magnitude larger. To determine the matrix rearrangements that allowed this amplification, we tracked the movements of collagen matrix surrounding two explants, again using glass beads as fiducial markers (Fig. 4; Video 3, available at http://www.jcb.org/cgi/content/full/jcb.200203069). As alignment occurred, beads located at the center of the strap moved little due to the near-symmetric pulling from opposed explants. Beads on the axis of the strap that were closer to one or the other of the explants did move toward their respective explant, but not much (<5% strain along the axis). This demonstrates that the collagen meshwork is relatively inextensible, consistent with the individual fibers having a high longitudinal stiffness (Wainwright, 1976). Indeed, over the course of the experiment, bead tracking showed that collagen fibers on the axis moved at only ~0.05 μm/min, much less than the 0.28 μm/min of collagen fibers early in the isolated explant experiment (Table I). However, consistent with our previous finding that the rate of collagen-versus-cell movement remains constant at 0.38 μm/min, the slow movement of collagen along the axis was complemented by a rapid 0.34-μm/min advancement of fibroblast processes from the explants, along the axis (Fig. 4, compare A and B). The slow rate of collagen movement was similar to that late in the single-explant experiment, indicating that the limiting strain of collagen matrix is rapidly reached between two explants, but is delayed when a solitary explant is surrounded by centimeters of matrix between it and the edge of the dish.

In comparison with the small axial movements on the strap between explants, beads in areas lateral to the strap were transported toward the axis 7-fold farther, >100 μm in 8 h, averaging 0.24 μm/min. Even in regions far removed from the strap or explants, beads start moving immediately upon cell spreading (Fig. 4 B); therefore, although fibroblasts are interacting with collagen fibers only locally, their effect is transmitted simultaneously throughout the surrounding collagen gel. The dramatic movement of collagen, perpendicular to the axis between the explants and into the forming strap, was unexpected, but was seen in all videos of gels populated with multiple explants.

Stability of the pattern

The tensile and compressive strains within patterned collagen gels are partially maintained by cell activity. Killing the cells by permeabilization with maitotoxin (Schilling et al., 1999) partially relieved the matrix strain (after a brief [<5 min] contraction of the explants, possibly due to an influx of calcium ions; Fig. 4 C). Measurements of the tracks of the six beads that moved laterally in Fig. 4 B revealed that maitotoxin reduced the matrix distortion by 58 ± 15% within 15 min. Similar results were obtained in two other bead-tracking experiments. The small tensile strain that develops along the axis of the strap was also partially relieved by maitotoxin (48 ± 19%, $n = 3$ straps). The relief of strain indicates that the matrix is elastic, and that during pattern formation the collagen fibers do not slide past each other: energy must be stored in the gel as tension within the strap or as compression near the explant. Killing cells by treatment with either maitotoxin or a detergent led also to only a partial decrease in strap anisotropy as measured by contrast analysis (Fig. 5).

The failure of the gel to rebound fully after cell death may be due to irreversible/stable fusion of collagen fibers drawn

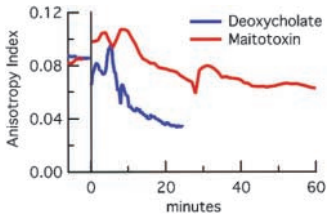

Figure 5. **Contrast analysis of pattern relaxation.** In two experiments, explants were embedded into collagen and allowed to form patterns for 8 h. At time 0, either maitotoxin or deoxycholate was added. In both, as cells die the anisotropy index decreases, but not to zero. With maitotoxin addition, there was a rapid contraction before the steady decline. As cells died there was little to focus on except for the densest aligned fibers in view. At minute 30, the microscope was refocused, causing the bump in anisotropy.

together during patterning (Guidry and Grinnell, 1986). To determine the most likely areas of collagen fusion, explants were embedded in collagen gels as in previous experiments, but were fixed after either 1 or 18 h. These samples were sectioned vertically along the axis between explants, stained with toluidine, and observed in bright field. Fibroblasts were initially round, and the collagen appeared as a loose, unorganized mesh (Fig. 6, A and B). After the 18 h incubation (Fig. 6, C and D), fibroblasts had remained near the interface between the upper and lower collagen layers, giving the explants a disk-like shape—round when viewed from above but flat. Collagen fibers were drawn in and compacted underneath the outer rim of this disk during patterning (Fig. 6 C). Within the strap (Fig. 6 D), long parallel fibers remained in the plane of section for distances >50 μm, confirming the alignment of collagen. Fourier analysis previously revealed that these aligned fibers in the strap region do become more closely packed over time (Fig. 2 D). Therefore, we attribute the stability of the strap pattern to collagen fusion within the strap itself and also in the compacted region near the explant rim. Ongoing fusion, which might zip together aligning fibers, may contribute to patterning but is unlikely to be its predominant driving force. If it were, we would expect collagen alignment to continue for some time even after cell death.

Discussion

Axial and lateral traction lead to lateral compression

We have reconciled the apparent temporal discrepancy between traction patterning and its cellular components by demonstrating that the orchestrated redistribution of collagen occurs on a time scale of minutes, consistent with the timescale of cell motility known from the study of migration. Now we can address the apparent spatial discrepancy: how can fibroblasts interacting only with local collagen molecules and moving them <10 μm, induce the immediate coordinated global rearrangement of collagen fibers almost 1,000 μm away, all along the strap and throughout the adjacent regions of the gel (Fig. 4)? The answer lies in understanding how tensile forces exerted by cells on their substrates drive the dramatic lateral compression of collagen into the forming strap. This somewhat counter-intuitive movement can be understood if the collagen gel is considered as an interconnected matrix or mesh, rather than as a collection of distinct fibers. If fibers were independent and could slide along each other, we would expect a lag phase between the spreading of cells and the movement of distant matrix markers, during which time the slack could be taken out of individual fibers. Also, we would expect neighboring beads to move at different speeds depending on whether or not they were attached to fibers originating at an explant. Instead, there was little or no lag, and the matrix with its associated beads, moved as a sheet (Fig. 4 B). Furthermore, releasing the matrix by killing the cells resulted in only a partial loss of collagen alignment (Figs. 4 C and 5). This is consistent with the collagen gel being a mechanically integrated meshwork of fibers

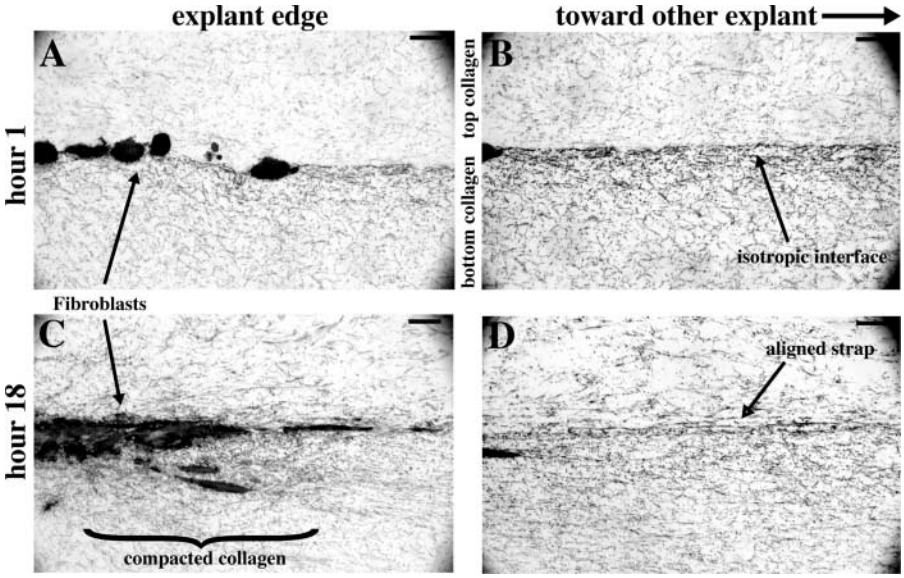

Figure 6. **Vertical section of strap.** Two explants of human periodontal ligament fibroblasts were embedded in collagen gels, fixed after 1 (A and B) or 18 h (C and D), and sectioned vertically, parallel to the strap. The opposing explant is to the right, out of these views. (A) Cells are initially round. (B) Between the explants, at the interface of the upper and lower layers of collagen, no long fibers are seen. This indicates that fibers are projecting in and out of the plane of section, consistent with the view of a coarse isotropic mesh when seen from above (Fig. 1). (C) After 18 h, cells are elongated and collagen fibers radiate from cell processes extending into the developed strap. Dense collagen has accumulated near the cells, especially below the explant. (D) Within the strap, long straight aligned fibers are seen remaining in the plane of section for longer than 50 μm, although randomly oriented fibers persist.

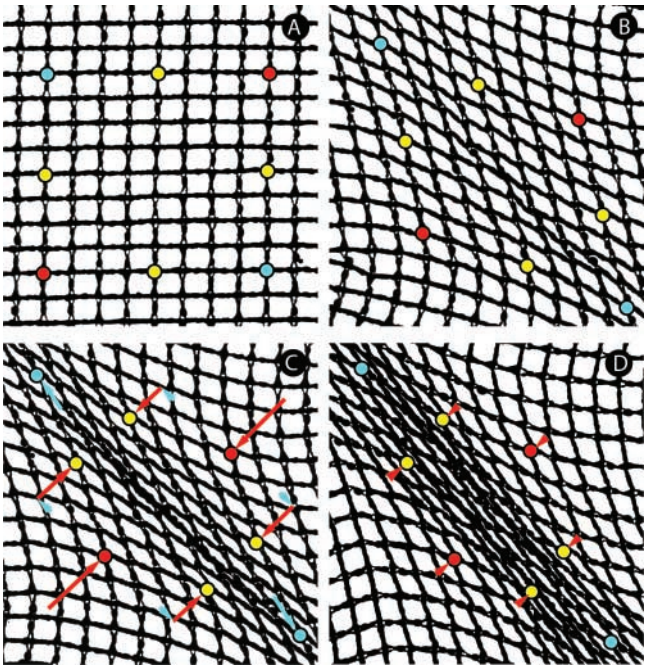

Figure 7. **Physical model of matrix movements.** A flexible yet inextensible mesh was imaged on a flatbed scanner. (A) Passive mesh, with reference points marked. (B) As tension was added from single points at the upper left and lower right corners, the mesh pattern became distorted, with square shapes elongating into diamonds as fibers aligned. (C) Further tension produced an aligned strap. Arrows show the mesh movements relative to the strap axis (parallel, blue; perpendicular, red). The tensile load resulted in a relatively small tensile strain, but a larger compressive displacement at a right angle. We term this feature of mesh geometry the orthogonal amplification of mesh distortion. (D) Pulling from multiple points adjacent to the axial corners increased the lateral draw of mesh and produced a broader strap.

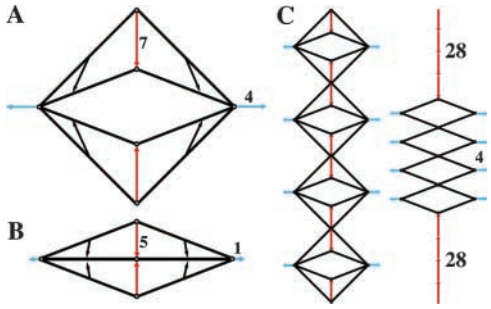

Figure 8. **Geometric model illustrating the principle of orthogonal amplification.** (A) Consider a square rhombus with strings for sides, hinges at the top and bottom corners, and pulleys at the right and left corners. The pulleys are maintained 24 units apart. Pulling the strings through the pulleys shortens each side by four units and pulls the upper and lower corners toward the horizontal axis by 7 units. (B) Further shortening the sides by only one unit is amplified into a five-unit vertical movement of the corners, compressing the rhombus into a line on the axis. Whereas the upper and lower corners move only vertically, points midway on the sides move vertically and horizontally. However, vertical movements dominate, and the direction of movement approaches pure vertical with progress toward the axis. (C) When four units are placed in parallel, the amplification is increased fourfold.

that branch and merge (Gross, 1961), due to the fact that adjacent fibers can fuse during gel polymerization (Birk et al., 1995), or when brought together (Guidry and Grinnell, 1986) during patterning.

We can model mesh behavior using a nylon net on a flatbed scanner (Fig. 7). Although the strings are flexible, they do not stretch, and crossed strings cannot slide across each other at their junctions. Initially, the strings run either horizontally or vertically, with right angles at their intersections, making square patterns. As the net is stretched from the upper left and lower right corners, the squares along the diagonal turn to diamonds, extending along the axis of strain and drawing the net in laterally toward the axis. With increased strain, the diamonds fully collapse, bringing strings into alignment along the axis of strain. This result is similar to that in a model from Weiss's (1934) classic exploration of the two-center effect. Whereas he presented the alignment produced when an elastic net is stretched out and then bunched from 360° into two foci, here we show that with an inextensible-fiber mesh, a small pull from only two points induces a large counter-intuitive redistribution of fibers. Measuring the distances between fiducial marks on our model mesh, we find that the points lateral to the axis of stretch (red) move almost twice the distance towards each other as the points on the axis (blue) move away from each other. At intermediate points (yellow), again the lateral component of displacement exceeds the axial. Pulling from multiple points near the corners instead of single points at the corners, does not lead to further axial strain, but does add to the lateral compression (Fig. 7 D), making the model more closely resemble Fig. 4.

Thus, axial tension induces small movements along the axis, but large movements at right angles to it. We term this phenomenon the orthogonal amplification of mesh distortion. To further explore the geometric principle, consider a square set on a corner (Fig. 8 A). If the two corners on the horizontal axis are held in place (analogous to traction units drawing in substrate), shortening the sides equally by a small amount, moves the upper and lower corners toward the horizontal axis by a large amount. As the sides become increasingly compressed toward the horizontal axis (Fig. 8 B), the amplification (the ratio of vertical to horizontal movement) becomes more dramatic. The trajectories of points on the sides become progressively vertical as they approach the axis. When multiple units are in parallel, the amplification is further increased (Fig. 8 C).

As demonstrated previously, collagen is drawn in from 360° around a solitary explant (Fig. 3). Therefore, we assume that the concerted rearrangement of collagen into a strap between two explants reflects input from both the axial and lateral components of traction. The lateral component of traction would obviously lead to a lateral movement of collagen into the strap; however, the nylon mesh model predicts that the pure axial component of traction also contributes substantially to the lateral movement of collagen. Thus orthogonal amplification helps to resolve the apparent spatial and temporal discrepancies discussed above, by explaining how the coupling of small tensile movements to large compressive movements can enable fibroblasts, that draw collagen slowly, to induce rapid long-reaching self-organization of the gel.

Conclusions and relevance

We have studied how cell traction leads to tissue-like patterns in collagen gels. Traction is the alter ego of migration; it is the engagement of the cell motility machinery, not for the primary purpose of transporting the cell, but instead for the distortion or rearrangement of surrounding matrix. Explant fibroblasts extend, attach to matrix, and contract, while maintaining their rear connections to neighbors or collagen fibers within the explant; and they advance at a constant rate in relation to the matrix, at a speed similar to that of fibroblast migration. This advancement is initially expressed as a centripetal traction of collagen in toward the explant until later, when tensile strain builds up in the gel and the cells begin to migrate away from the explant. By maintaining proximity to one another, periodontal ligament fibroblasts in the explant function collectively as a traction unit. Furthermore, the strap pattern they produce is not simply a transient distortion, but is a stable remodeling of matrix that is only partially maintained by cell activity. These fibroblasts may function similarly in vivo, where they occupy 25% of the tissue volume, maintain contact with each other through ~20 gap- and adherence-type junctions (Beertsen et al., 2000), and are oriented parallel to the axis of tissue strain and collagen alignment, and may contribute to the tensional homeostasis of the tissue.

Orthogonal amplification represents a method through which slow-moving cells might drive the rapid tissue movements required during development and wound healing. For example, traction by fibroblasts oriented parallel to the surface of a bone might draw matrix laterally onto the surface making a periosteum-like sheet (Stopak and Harris, 1982; Stopak et al., 1985). There may also be intracellular analogues to the phenomenon. One intriguing candidate is in the canoe-shaped fish keratocyte. This cell migrates rapidly and persistently (Euteneuer and Schliwa, 1984) even though the largest force it exerts on its substrate is perpendicular to the direction of migration (Lee et al., 1994; Oliver et al., 1994). In these cells, myosin contracting the actin cortical mesh in one direction might drive the rapid displacement of the cell in the orthogonal direction. Indeed, two features of keratocyte morphology support this view: the actin strap seen arcing across the cell, anterior to the nucleus (Svitkina et al., 1997), and the fact that the force exerted on the substrate under the cell is directed from the front and rear of the cell toward this strap (Galbraith and Sheetz, 1999). By anchoring to the substrate on one side of the actin strap (Cramer et al., 1997) and detaching on the other side (Anderson and Cross, 2000), the cell could bias its lateral movement toward one direction. The geometries of various biological meshes and the force-generating components that move them need to be further analyzed in order to assess the extent to which orthogonal amplification might help drive movements in vivo.

Materials and methods

Experimental setup

Explants of primary neonatal mouse dermal fibroblasts and primary human periodontal ligament fibroblasts were embedded in collagen gels as previously described (Stopak and Harris, 1982). Acid-solublized type I collagen (Cohesion Technologies) was neutralized and diluted to 1.5 mg/ml in Hepes-buffered low-glucose DME plus penicillin-streptomycin and 10% FBS (all reagents from GIBCO BRL). 475 μl of this mixture was added to a 35-mm culture dish with a 1.5 coverslip floor (Mattek), and allowed to polymerize overnight at 37°C, normal atmosphere.

The following morning, a 10-cm dish of subconfluent cells was trypsinized and washed in media. Cells were pelleted then resuspended in 50 μl of unpolymerized collagen mixture, transferred to a 650-μl microcentrifuge tube, and centrifuged at 265 × *g* for 20 s. After the supernatant was aspirated, 4 μl of collagen mixture was added to aid pipetting. Explants, consisting of 0.2 μl of cell suspension were pipetted atop the polymerized collagen gel, spaced ~1 mm apart. Analysis of fixed and sectioned explants revealed that each explant consists of ~4,000 cells (unpublished data).

Cells were allowed to settle and attach to the collagen matrix for 1 h at 37°C, after which 525 μl of 1.85 mg/ml collagen mixture was added. The final collagen concentration in the total sample was 1.7 mg/ml. In some experiments, 6- to 16-μm diameter glass spheres (Mo-Sci) were suspended in the second collagen mixture; these settled to the cell level and served as reference points for tracking. The dish was immediately enclosed in a humid 37°C chamber (custom built with parts from Cell MicroControls) on the microscope stage. Cells remain viable and active in this setup for at least 24 h.

Microscopy

Images were obtained on a Diaphot 200 inverted microscope (Nikon), using a 10× phase contrast objective, a 0.6× video coupler (Diagnostic Instruments), and a MicroMax-1300Y cooled CCD camera (Princeton Instruments), driven by Metamorph imaging software (Universal Imaging). Images were obtained once per minute, and raw data were stored as uncompressed 8-bit digital tiff files.

Samples to be sectioned were prepared as above, but were left in a 37°C incubator for 1 or 18 h to allow pattern formation. Samples were fixed in 2% paraformaldehyde, 2.5% EM grade glutaraldehyde, and 0.1 M cacodylate buffer, pH 7.35, for 4–24 h at 4°C. After thorough washing, samples were post-fixed with 1% OsO_4 in 0.1 M cacodylate buffer for 90 min at room temperature. They were then dehydrated to 70% ethanol and stained en bloc with 3% uranyl acetate in 70% ethanol for 1 h in the dark. Dehydration was continued to absolute alcohol, and then samples were infiltrated overnight with Spurrs low-viscosity embedding resin and polymerized for 48 h at 70°C. 1-μm sections were cut and stained with 1% toluidine blue in 1% sodium borate. These were imaged in brightfield on an Axiovert 200 with a 40× plan Neofluar oil-immersion objective (Zeiss), with a Spot CCD camera (Diagnostic Instruments) driven by IPLab software.

Image analysis

Stacks of sequential images were prepared for analysis, and Fourier transformations were performed and power spectra generated, using NIH Image software. For each contrast analysis, all images were rotated so that the strap forming between two explants was horizontal. A region of the strap, usually 60 × 360 pixels in size, at 1.1 μm per pixel, was imported into Igor Pro (WaveMetrics) for measurement of gel anisotropy. A program was written that digitally chops each rectangular strap image into 60 × 60 pixel squares and then slices each square into lines, thereby producing 360 horizontal (parallel to the strap) and 360 vertical (perpendicular to the strap) lines, each 60 pixel values long, with each value representing the brightness on a scale from 0 to 255. For each line, the algorithm calculates the contrast, defined as

$$C = \frac{\sigma}{\mu}$$

where σ is the standard deviation for the pixel values, and μ is the mean pixel value. For each image, a mean parallel contrast and a mean perpendicular contrast were calculated

$$C_{\parallel} = \frac{1}{n}\sum_{i=1}^{n} C_{\parallel}^{i}$$

and

$$C_{\perp} = \frac{1}{n}\sum_{i=1}^{n} C_{\perp}^{i}$$

where $C_{\parallel}$ and $C_{\perp}$; are the parallel and perpendicular contrasts, respectively, and n is the number of lines analyzed per image in each direction—usually 360. Finally, an anisotropy index was calculated for each image.

$$AI = \frac{C_{\perp} - C_{\parallel}}{\frac{1}{2}(C_{\perp} + C_{\parallel})}.$$

Online supplemental material

The online version of this article includes three videos (available at http://www.jcb.org/cgi/content/full/jcb.200203069) corresponding to Figs 1, 3, and 4. Video 1 (Fig. 1) shows three explants of mouse neonatal skin fibroblasts embedded in a collagen gel and filmed in phase contrast for 8 h. Bar, 100 μm. Video 2 (Fig. 3) shows a solitary explant of human periodontal ligament fibroblasts filmed in phase contrast for 18 h. Tracking glass beads dispersed at the level of the cells allows assessment of collagen movements. Bar, 100 μm. Video 3 (Fig. 4) shows two explants of human periodontal ligament fibroblasts. Eight fiducial glass beads are marked in red. Compressive movements dominate axial movements during strap formation. After 8 h, maitotoxin is added to kill the cells, releasing 1/2 to 2/3 of the matrix strain. Bar, 100 μm.

We thank Drs. M. Landolfa, K. Neugebauer, and E. Tanaka for their comments on an earlier version of the manuscript, Dr. W. Schief for help with Igor programming, and A.K. Harris for his encouragement and expertise during the initial formulation of this project.

This research was supported by the National Institute of Dental and Craniofacial Research (RS) and the Max Planck Society (J. Howard).

Submitted: 14 March 2002
Revised: 25 April 2002
Accepted: 30 April 2002

References

Anderson, K.I., and R. Cross. 2000. Contact dynamics during keratocyte motility. *Curr. Biol.* 10:253–260.

Balaban, N.Q., U.S. Schwarz, D. Riveline, P. Goichberg, G. Tzur, I. Sabanay, D. Mahalu, S. Safran, A. Bershadsky, L. Addadi, and B. Geiger. 2001. Force and focal adhesion assembly: a close relationship studied using elastic micropatterned substrates. *Nat. Cell Biol.* 3:466–472.

Beertsen, W., C.A. McCulloch, and J. Sodek. 2000. The periodontal ligament: a unique, multifunctional connective tissue. *Periodontology.* 13:20–40.

Bell, E., B. Ivarsson, and C. Merrill. 1979. Production of a tissue-like structure by contraction of collagen lattices by human fibroblasts of different proliferative potential in vitro. *Proc. Natl. Acad. Sci. USA.* 76:1274–1278.

Bellows, C.G., A.H. Melcher, and J.E. Aubin. 1981. Contraction and organization of collagen gels by cells cultured from periodontal ligament, gingiva and bone suggest functional differences between cell types. *J. Cell Sci.* 50:299–314.

Bellows, C.G., A.H. Melcher, and J.E. Aubin. 1982. Association between tension and orientation of periodontal ligament fibroblasts and exogenous collagen fibers in collagen gels in vitro. *J. Cell Sci.* 58:125–138.

Beningo, K.A., M. Dembo, I. Kaverina, J.V. Small, and Y.L. Wang. 2001. Nascent focal adhesions are responsible for the generation of strong propulsive forces in migrating fibroblasts. *J. Cell Biol.* 153:881–888.

Birk, D.E., M.V. Nurminskaya, and E.I. Zycband. 1995. Collagen fibrillogenesis in situ: fibril segments undergo post-depositional modifications resulting in linear and lateral growth during matrix development. *Dev. Dyn.* 202:229–243.

Bray, D. 2001. Cell movements: from molecules to motility. Garland Publishing, New York. 372 pp.

Brown, R.A., R. Prajapati, D.A. McGrouther, I.V. Yannas, and M. Eastwood. 1998. Tensional homeostasis in dermal fibroblasts: mechanical responses to mechanical loading in three-dimensional substrates. *J. Cell Physiol.* 175:323–332.

Cramer, L.P., M. Siebert, and T.J. Mitchison. 1997. Identification of novel graded polarity actin filament bundles in locomoting heart fibroblasts: implications for the generation of motile force. *J. Cell Biol.* 136:1287–1305.

Eastwood, M., D.A. McGrouther, and R.A. Brown. 1994. A culture force monitor for measurement of contraction forces generated in human dermal fibroblast cultures: evidence for cell-matrix mechanical signaling. *Biochim. Biophys. Acta.* 1201:186–192.

Euteneuer, U., and M. Schliwa. 1984. Persistent, directional motility of cells and cytoplasmic fragments in the absence of microtubules. *Nature.* 310:58–61.

Fray, T.R., J.E. Molloy, M.P. Armitage, and J.C. Sparrow. 1998. Quantification of single human dermal fibroblast contraction. *Tissue Eng.* 4:281–291.

Galbraith, C.G., and M.P. Sheetz. 1999. Keratocytes pull with similar forces on their dorsal and ventral surfaces. *J. Cell Biol.* 147:1313–1324.

Gross, J. 1961. Collagen. *Sci. Am.* 204:120–130.

Guidry, C., and F. Grinnell. 1985. Studies on the mechanism of hydrated collagen gel reorganization by human skin fibroblasts. *J. Cell Sci.* 79:67–81.

Guidry, C., and F. Grinnell. 1986. Contraction of hydrated collagen gels by fibroblasts: evidence for two mechanisms by which collagen fibrils are stabilized. *Coll. Relat. Res.* 6:515–529.

Harris, A.K., P. Wild, and D. Stopak. 1980. Silicone rubber substrata: a new wrinkle in the study of cell locomotion. *Science.* 208:177–179.

Harris, A.K., D. Stopak, and P. Wild. 1981. Fibroblast traction as a mechanism for collagen morphogenesis. *Nature.* 290:249–251.

Kaverina, I., O. Krylyshkina, and J.V. Small. 1999. Microtubule targeting of substrate contacts promotes their relaxation and dissociation. *J. Cell Biol.* 146:1033–1044.

Lee, J., M. Leonard, T. Oliver, A. Ishihara, and K. Jacobson. 1994. Traction forces generated by locomoting keratocytes. *J. Cell Biol.* 127:1957–1964.

Loisel, T.P., R. Boujemaa, D. Pantaloni, and M.F. Carlier. 1999. Reconstitution of actin-based motility of Listeria and Shigella using pure proteins. *Nature.* 401:613–616.

Machesky, L.M., S.J. Atkinson, C. Ampe, J. Vandekerckhove, and T.D. Pollard. 1994. Purification of a cortical complex containing two unconventional actins from Acanthamoeba by affinity chromatography on profilin-agarose. *J. Cell Biol.* 127:107–115.

Oliver, T., J. Lee, and K. Jacobson. 1994. Forces exerted by locomoting cells. *Semin. Cell Biol.* 5:139–147.

Schilling, W.P., W.G. Sinkins, and M. Estacion. 1999. Maitotoxin activates a nonselective cation channel and a P2Z/P2X(7)-like cytolytic pore in human skin fibroblasts. *Am. J. Physiol.* 277:C755–C765.

Smilenov, L.B., A. Mikhailov, R.J. Pelham, E.E. Marcantonio, and G.G. Gundersen. 1999. Focal adhesion motility revealed in stationary fibroblasts. *Science.* 286:1172–1174.

Stopak, D., and A.K. Harris. 1982. Connective tissue morphogenesis by fibroblast traction. I. Tissue culture observations. *Dev. Biol.* 90:383–398.

Stopak, D., N.K. Wessells, and A.K. Harris. 1985. Morphogenetic rearrangement of injected collagen in developing chicken limb buds. *Proc. Natl. Acad. Sci. USA.* 82:2804–2808.

Svitkina, T.M., A.B. Verkhovsky, K.M. McQuade, and G.G. Borisy. 1997. Analysis of the actin-myosin II system in fish epidermal keratocytes: mechanism of cell body translocation. *J. Cell Biol.* 139:397–415.

Svitkina, T.M., and G.G. Borisy. 1999. Arp2/3 complex and actin depolymerizing factor/cofilin in dendritic organization and treadmilling of actin filament array in lamellipodia. *J. Cell Biol.* 145:1009–1026.

Theriot, J.A., and T.J. Mitchison. 1992. Comparison of actin and cell surface dynamics in motile fibroblasts. *J. Cell Biol.* 119:367–377.

Vasiliev, J.M., I.M. Gelfand, L.V. Domnina, O.Y. Ivanova, S.G. Komm, and L.V. Olshevskaja. 1970. Effect of colcemid on the locomotory behavior of fibroblasts. *J. Embryol. Exp. Morphol.* 24:625–640.

Wainwright, S.A. 1976. Mechanical design in organisms. Edward Arnold, London. 423 pp.

Wang, Y.L. 1985. Exchange of actin subunits at the leading edge of living fibroblasts: possible role of treadmilling. *J. Cell Biol.* 101:597–602.

Weiss, P. 1934. In vitro experiments on the factors determining the course of the outgrowing nerve fiber. *J. Exp. Zool.* 68:393–448.

Yamato, M., E. Adachi, K. Yamamoto, and T. Hayashi. 1995. Condensation of collagen fibrils to the direct vicinity of fibroblasts as a cause of gel contraction. *J. Biochem.* 117:940–946.